

Pit Membrane Porosity and Water Stress-Induced Cavitation in Four Co-Existing Dry Rainforest Tree Species

Brendan Choat^{1*}, Marilyn Ball, Jon Luly, and Joseph Holtum

Department of Tropical Plant Science (B.C., J.H.) and Department of Tropical Environmental Studies and Geography (J.L.), James Cook University, Townsville, Queensland, Australia, 4811; and Research School of Biological Sciences, Australian National University, Canberra, Australian Capital Territory, Australia, 2601 (B.C., M.B.)

Aspects of xylem anatomy and vulnerability to water stress-induced embolism were examined in stems of two drought-deciduous species, *Brachychiton australis* (Schott and Endl.) A. Terracc. and *Cochlospermum gillivraei* Benth., and two evergreen species, *Alphitonia excelsa* (Fenzl) Benth. and *Austromyrtus bidwillii* (Benth.) Burret., growing in a seasonally dry rainforest. The deciduous species were more vulnerable to water stress-induced xylem embolism. *B. australis* and *C. gillivraei* reached a 50% loss of hydraulic conductivity at -3.17 MPa and -1.44 MPa, respectively; a 50% loss of hydraulic conductivity occurred at -5.56 MPa in *A. excelsa* and -5.12 MPa in *A. bidwillii*. To determine whether pit membrane porosity was responsible for greater vulnerability to embolism (air seeding hypothesis), pit membrane structure was examined. Expected pore sizes were calculated from vulnerability curves; however, the predicted inter-specific variation in pore sizes was not detected using scanning electron microscopy (pores were not visible to a resolution of 20 nm). Suspensions of colloidal gold particles were then perfused through branch sections. These experiments indicated that pit membrane pores were between 5 and 20 nm in diameter in all four species. The results may be explained by three possibilities: (a) the pores of the expected size range were not present, (b) larger pores, within the size range to cause air seeding, were present but were rare enough to avoid detection, or (c) pore sizes in the expected range only develop while the membrane is under mechanical stress (during air seeding) due to stretching/flexing.

Xylem cavitation and embolism are recognized as major constraints affecting plants regularly exposed to water stress (Tyree and Sperry, 1989; Milburn, 1993). Water in the xylem is under negative pressure, or tension, i.e. it is held in a metastable state, below its vapor pressure, a condition that increases the likelihood of cavitation occurring (Oertli, 1971; Pickard, 1981). Cavitation is the process whereby a vapor phase is introduced to the xylem water column, creating an embolism. Embolisms are gas bubbles consisting initially of water vapor and later air, which become trapped within xylem conduits. Because of its inability to transmit tension, the vapor phase limits the volume flow of water through the conduit, reducing the plant's capacity to deliver water to the canopy (Meinzer et al., 2001). Plants must minimize this disruption to water transport to avoid effects on leaf water status that may result in limitations on stomatal conductance and photosynthesis.

The structure of xylem vessels is seen as an important factor in determining the occurrence of water

stress-induced cavitation (Zimmermann, 1983). Xylem vessels are bounded by pit membranes, through which water must pass to move from one vessel to the next. Pit membranes are the degraded primary cell walls and middle lamella of the vessels and are composed of tightly inter-woven cellulose microfibrils in a matrix of hemicellulose and pectin polysaccharides (Dixon, 2000). Pit membranes act as finely porous filters, allowing the free passage of water and nutrients while limiting the passage of air bubbles, pathogens, and particles between the adjacent xylem vessels (Crombie et al., 1985).

It is generally accepted that water stress-induced embolisms result from heterogenous nucleation of cavitation within xylem conduits (Pickard, 1981; Tyree et al., 1994). Empirical evidence indicates that the primary cause of water stress-induced embolism is the penetration of air through pit membranes between adjacent vessels, a process known as the "air seeding" (Zimmermann, 1983; Sperry and Tyree, 1988). A brief description of the process follows: When cavitation occurs, the vessel fills with water vapor. The vapor phase will expand within the vessel until it reaches the finely porous pit membranes where it will be stopped by the surface tension of the water. The embolized vessel will now be at the vapor pressure of water (2.3 kPa absolute pressure), whereas adjacent, functional vessels contain water

¹ Present address: Department of Organismic and Evolutionary Biology, Biological Laboratories, Harvard University, 16 Divinity Avenue, Cambridge, MA 02138.

* Corresponding author; e-mail bchoat@oeb.harvard.edu; fax 617-496-5854.

Article, publication date, and citation information can be found at www.plantphysiol.org/cgi/doi/10.1104/pp.014100.

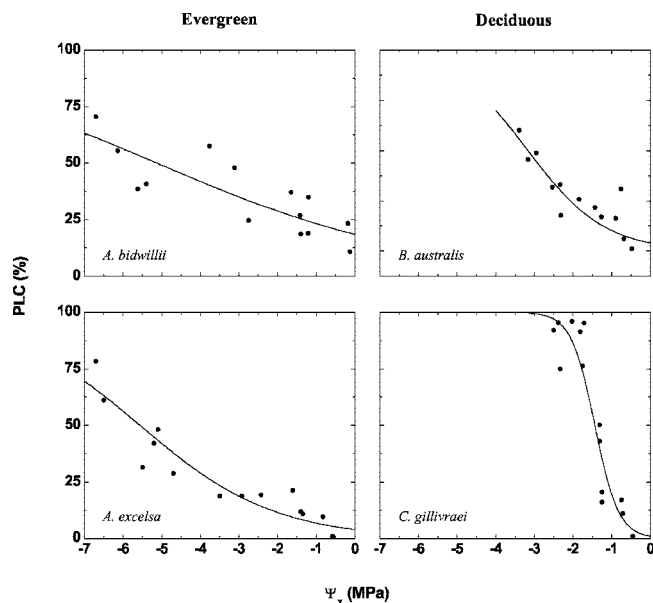


Figure 1. Vulnerability curves in species of contrasting leaf phenology showing PLC versus Ψ_x in excised air-dried stem segments. Each point represents PLC for single branch. Vulnerability curves were obtained by fitting the exponential sigmoidal equation $PLC = 100 / (1 + \exp\{a[\Psi_x - b]\})$, to the data, where a describes the slope of the curve and b is the Ψ_x at which a PLC of 50 occurs (Pammenter and Vander Willigen, 1998). Values for a , b , and r^2 are given in Table I.

under tension. The pressure in the embolized vessel will slowly increase to atmospheric as air diffuses into the embolism from surrounding cells. The gas bubble will be trapped at the pit membrane pores until the pressure difference between the vessels becomes great enough for a small bubble to be drawn through a pore into a functional vessel where it may nucleate a new cavitation.

The pressure gradient (ΔP) in MPa required to pull an air bubble through a pit membrane pore of a given size can be calculated from a modified form of the capillary equation:

$$\Delta P = 4 (\tau \cos\theta / D) \tag{1}$$

where D (micrometer) represents the diameter of the pit membrane pore and τ (Newtons per meter) is the surface tension of water. The contact angle (θ) between the air water interface and the pit membrane is assumed to be 0° . The implication of this relationship for plant structure is that xylem vessels with larger pit membrane pores will be more vulnerable to water stress-induced embolism than vessels with smaller pores.

This study relates vulnerability to water stress-induced embolism to selected anatomical characteristics of four coexisting tree species from seasonally dry rainforest in northern Australia. Two of the species are deciduous, *Brachychiton australis* (Schott and Endl.) A. Terracc. and *Cochlospermum gillivraei* Benth., and shed their leaves with the onset of drought, whereas the other two species are evergreens, *Alphi-*

tonia excelsa (Fenzl) Benth. and *Austromyrtus bidwillii* (Benth.) Burret., which maintain a canopy throughout the dry season. It is hypothesized that the evergreen species will be less vulnerable to embolism than the deciduous species and that this difference in vulnerability will be reflected in the morphology of the xylem vessels. In particular it is expected that inter-specific differences in pit membrane porosity will be observed and that the more vulnerable species will exhibit measurably larger pore sizes.

RESULTS

Vulnerability to Embolism

There were inter-specific differences in vulnerability to water stress-induced embolism, with deciduous species suffering a greater percentage loss of hydraulic conductivity (k_h ; PLC) for a given decline in xylem water potential (Ψ_x) than evergreen species (Fig. 1). This is shown by two coefficients: (a) the steeper slopes of vulnerability curves for deciduous species (coefficient a ; Table I); and (b) the xylem tension (Ψ_x) at which a PLC of 50 (PLC₅₀) occurred (coefficient b ; Table I) was more negative in evergreen species. Of the deciduous species, *C. gillivraei* was the most susceptible to embolism, with a PLC₅₀ occurring at -1.44 MPa, although some of the samples tested had suffered much greater PLC by this point. A PLC₅₀ occurred at -3.17 MPa for *B. australis*. The evergreen species had more gradual curves, with PLC₅₀ occurring at -5.56 MPa for *A. excelsa* and -5.12 MPa for *A. bidwillii*, respectively.

Vessel Anatomy

The deciduous species possessed significantly wider xylem vessels ($P < 0.001$) than the evergreen species (Table II). *C. gillivraei* had the widest with a mean vessel diameter of $104.56 \mu m$, followed by *B. australis* with $87.46 \mu m$. The evergreen species had narrower vessels with mean diameters of $47.04 \mu m$ and $32.03 \mu m$ for *A. excelsa* and *A. bidwillii*, respectively. The evergreen species *A. bidwillii* had the greatest maximum vessel length (0.37 m), longer than those of the two deciduous species (Table II).

Pit Membrane Porosity

The average maximum pore diameter in pit membranes was calculated for the ΔP producing a PLC of

Table I. Values of coefficients a and b from Equation 2, where a describes the slope of vulnerability curves presented in Figure 1 and b is the Ψ_x at which a PLC of 50 occurs

The r^2 values are given for each of the curves fitted in Figure 1.

Species	a	b	r^2
<i>A. bidwillii</i>	0.29	-5.12	0.65
<i>A. excelsa</i>	0.57	-5.56	0.87
<i>B. australis</i>	1.01	-3.17	0.78
<i>C. gillivraei</i>	3.27	-1.44	0.88

Table II. Maximum and mean vessel diameter (D) and maximum vessel length (L) in each species

Measurements diameter were made of three branches from each of three trees for each species ($n = 9$). Measurements of vessel length were made on four to five branches ($n = 4-5$). SE in parentheses.

Species	Max D	Mean D	Max L
	μm		m
<i>A. bidwillii</i>	41.45 (1.88)	32.03 (1.05)	0.37 (0.04)
<i>A. excelsa</i>	71.59 (1.03)	47.04 (1.30)	0.20 (0.02)
<i>B. australis</i>	148.11 (18.01)	87.46 (7.66)	0.33 (0.04)
<i>C. gillivraei</i>	166.94 (13.89)	104.56 (8.54)	0.34 (0.02)

50 using Equation 1 (Table III). Values given in Table III should be characteristic of maximum pit membrane pore diameters of branches used to measure vulnerability to embolism in each species. Pore diameters calculated for *A. excelsa* and *A. bidwillii* were 50 and 60 nm, respectively. The values for the more vulnerable deciduous species were 90 nm for *B. australis* and 200 nm for *C. gillivraei*.

Scanning electron micrographs of inter-vessel pit membranes did not reveal pores of the size predicted from vulnerability curves and the air seeding hypothesis (Fig. 2). Although many of the membranes viewed were damaged in sectioning or preparation, between 30 and 50 intact membranes were located in each species. At 35,000 to 50,000 \times magnification, the microfibrillar nature of the membranes was readily apparent.

Perfusion of gold colloid particles enabled a bracketing of membrane pore size. Visual inspection of perfusate indicated that 5-nm particles had penetrated pit membranes in all species. This was easily discernable from the discoloration of samples. In contrast, samples from branches perfused with 20-nm particles were clear. Analysis of perfusate by inductively coupled plasma mass spectroscopy (ICP-MS) confirmed that gold particles from 5-nm suspensions passed through the membranes of the four species. However, this sensitive technique also revealed that in samples *C. gillivraei* and *A. excelsa*, a small proportion (≈ 100 times less than 5-nm samples) of particles from 20-nm suspensions had penetrated pit membranes. No gold was detected in perfusate from 20-nm suspensions in *B. australis* and *A. bidwillii*. This information was derived in a quantitative manner from comparison of perfusate from samples with concentration standards. Representative graphs for

Table III. Pressure difference at PLC₅₀ (ΔP) and inter-vessel pit membrane pore diameter (D) calculated from Equation 1

Species	ΔP	Pore D
	MPa	nm
<i>A. bidwillii</i>	5.12	60
<i>A. excelsa</i>	5.56	50
<i>B. australis</i>	3.17	90
<i>C. gillivraei</i>	1.43	200

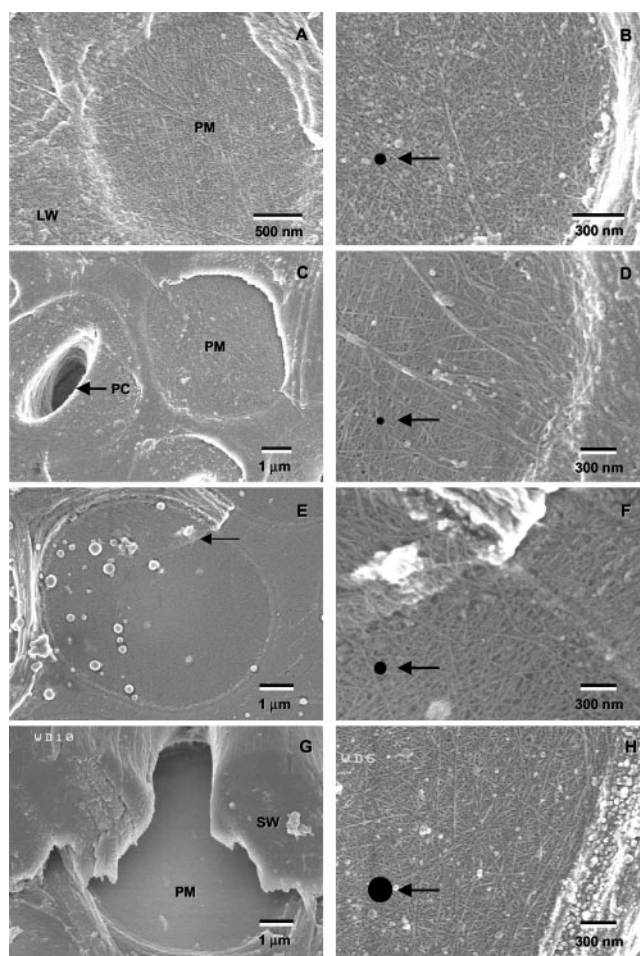


Figure 2. Scanning electron micrographs of inter-vessel pit membranes in each of the species. Each picture shows a longitudinal section of xylem tissue in which one secondary wall has been partially or fully removed to reveal pit membranes. Micrographs in the right column show higher resolution images in which the cellulose microfibrillar structure of membranes is clearly visible. Black dots shown in the right column represent circular pores of the size calculated for each species in Table III. A, Intact membranes (PM) of *A. bidwillii* with cellulose microfibrils visible ($\times 35,000$). The surrounding wall has been impregnated with lignin (LW), and microfibrils cannot be discerned. B, Closer view ($\times 50,000$) of pit membrane in *A. bidwillii*. C, Intact membrane (PM) and torn membrane revealing underlying pit channel (PC) in *A. excelsa* ($\times 10,000$). D, Detail of pit membrane in *A. excelsa* ($\times 35,000$) with margin of membrane visible to right side of micrograph. E, Pit membranes of *B. australis* ($\times 11,000$). Overlapping layers of microfibrils are visible at the top of the membrane in the center of the micrograph (arrow). F, Detail of membrane in *B. australis* showing closer view of overlapping primary wall layers ($\times 35,000$). G, Pit membrane (PM) of *C. gillivraei* with overarching secondary walls (SW; $\times 11,000$). H, Closer view of pit membrane in *C. gillivraei* at ($\times 35,000$). Margin of membrane and secondary wall is visible on right side of micrograph.

gold counts of a 5-nm sample, a 20-nm sample, and the concentration standard ($5 \mu\text{L L}^{-1}$ Au in suspension) are shown in Figure 3. Possible explanations for the penetration of a small proportion of particles from 20-nm suspensions are dealt with in the discussion.

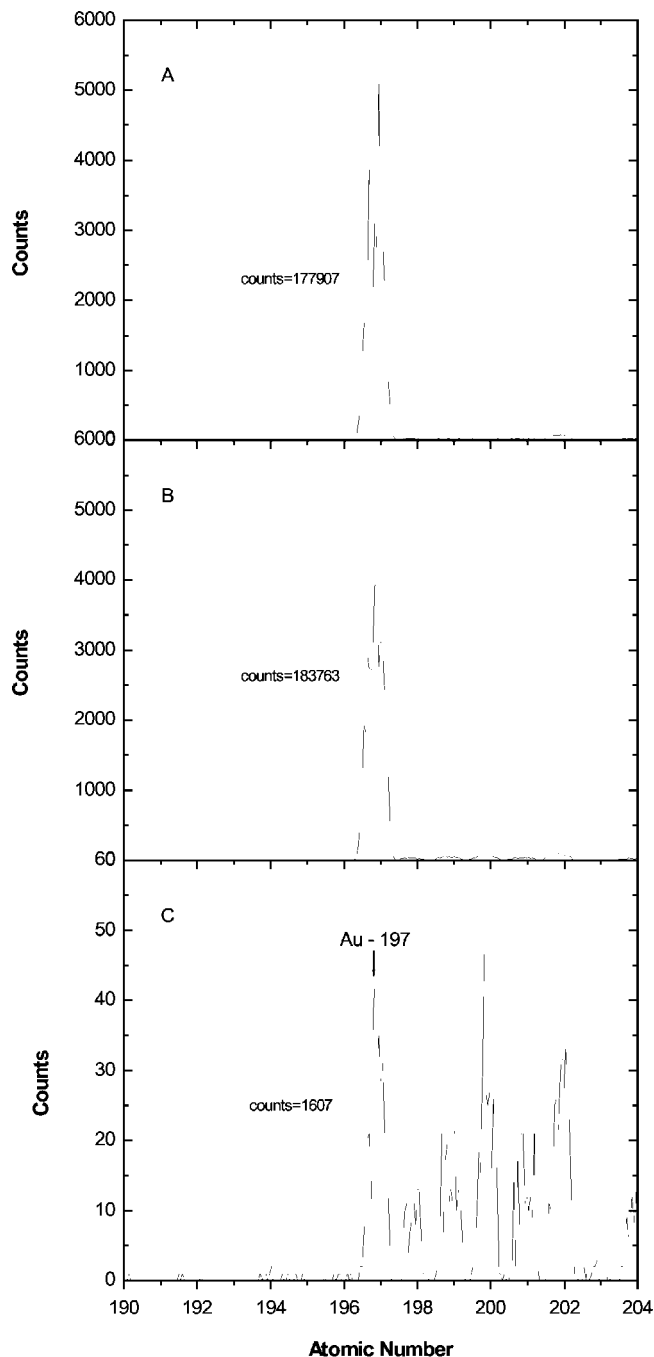


Figure 3. Detection of gold (Au) in perfusate using ICP-MS. Graphs show integrated counts of gold for concentration standard (A; $5 \mu\text{L L}^{-1}$ gold colloid in suspension), representative sample of 5-nm gold colloid perfusate from *C. gillivraei* (B), and representative sample of 20-nm gold colloid perfusate from *C. gillivraei* (C). Note the scale of y axis for 20-nm sample differs from 5-nm sample and concentration standard.

Longitudinal sections through the xylem tissue of each of the species demonstrated that the 20-nm gold particles were being trapped at inter-vessel pit membranes (Fig. 4, A, C, E, and G). The sections show a heavy accumulation of gold particles at the pit mem-

branes and in the pit cavities of adjacent xylem vessels. In contrast, sections through samples that were perfused with 5 nm of gold show little accumulation of particles at the pit membranes (Fig. 4, B, D, F, and H).

DISCUSSION

The four species examined in this study were predicted to differ in their vulnerability to embolism and xylem anatomy, specifically the diameter of pit membrane pores. Vulnerability curves indicated that the two deciduous species were more susceptible to water stress-induced embolism than coexisting evergreens (Fig. 1). Calculated values for pit membrane pore sizes based on the air seeding hypothesis (Table III) are accordingly smaller for the less vulnerable evergreen species; predicted mean pore sizes ranged between 50 nm for *A. excelsa* and 200 nm for *C. gillivraei*. However, the results of the present study did not confirm the existence of pores above 20 nm in diameter in pit membranes or the expected inter-specific variation in pore size.

Although pores of the predicted size range were not detected by scanning electron microscopy (SEM), it is possible that the structure of pit membranes was altered during the sectioning and preparation of the samples. The cellulose microfibrils of pit membranes are embedded in a highly hydrated matrix of pectin polysaccharides, which is roughly 75% water by mass (Dickson, 2000). During air drying, the arrangement of microfibrils may have changed causing pores originally present to be obscured, although it is also possible that tissue shrinkage could cause pores to become larger than they originally were. Shane et al. (2000) found that tissue drying could produce large holes in the pit membranes of maize (*Zea mays*) roots. Nevertheless, a number of other studies have related pit membrane porosity to cavitation threshold using SEM (Sperry and Tyree, 1988; Sperry et al., 1991; Alder et al., 1996; Harvey and van den Driessche, 1997). All studies stress the difficulty in discerning the difference between naturally occurring pores and artifactual damage caused during sectioning and preparation.

In the present study, SEM observations were consistent with particle perfusion experiments using colloidal gold, which indicated that the vast majority of pit membranes in the samples tested would not allow air seeding to occur at the pressure differences corresponding to a PLC_{50} in each species (Table III). This finding is not unprecedented in angiosperm species. Shane et al. (2000) determined that the pore size of pit membranes in maize roots were close to 5 nm. Cronshaw (1960) stated that colloidal carbon and gold particles (64 nm) did not cross pit membranes of *Eucalyptus regnans*, but he did not attempt experiments with smaller size particles. A study of xylem tissue in several hardwood species revealed inter-

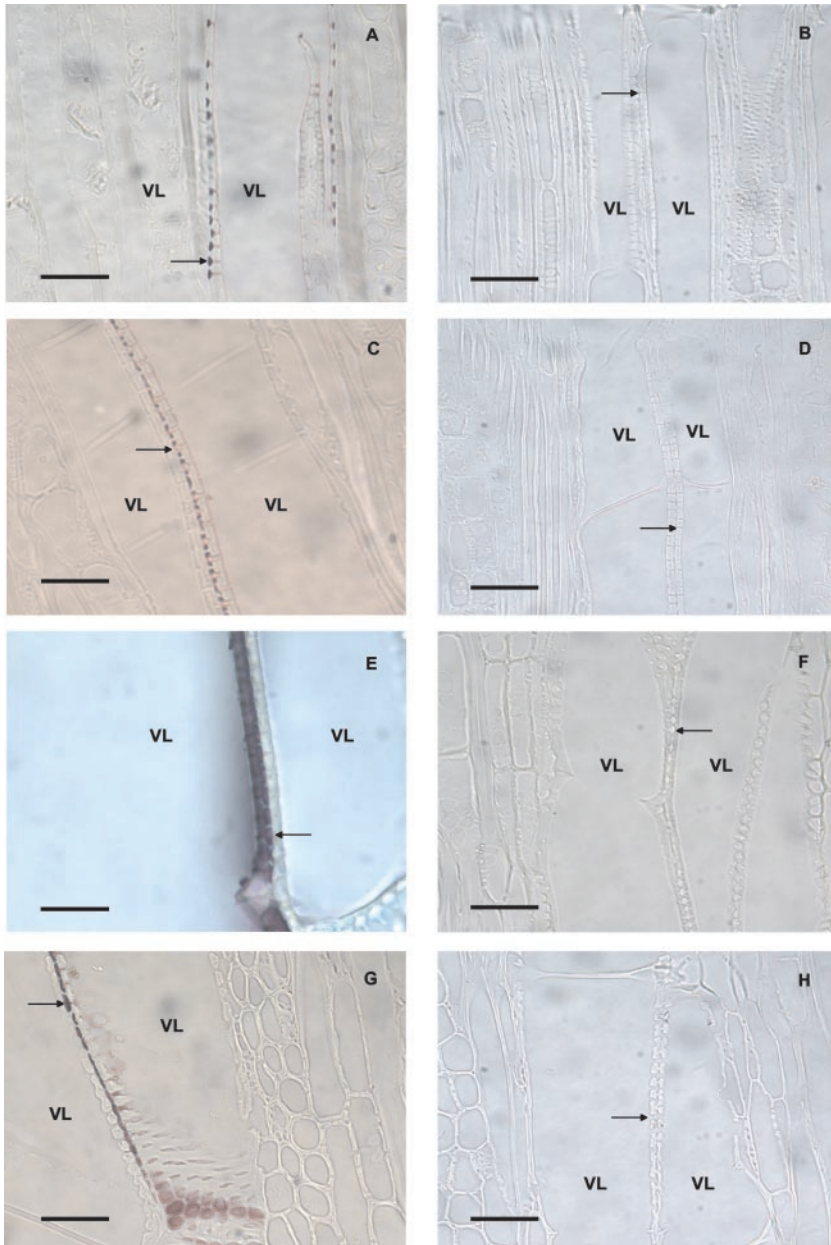


Figure 4. Light micrographs show tangential longitudinal sections through the xylem tissue of each species after perfusing branch segments with gold colloid suspensions. *A. bidwillii* (A and B), *A. excelsa* (C and D), *B. australis* (E and F), and *C. gillivraei* (G and H). All micrographs show two adjacent xylem vessels, with vessel lumens labeled VL. Pictures in the left column show branches that have been perfused with suspensions containing 20-nm gold colloids (A, C, E, and G). Gold particles have accumulated at inter-vessel pit membranes (arrows) and in pit cavities of each species. Stem sections shown in the right column have been perfused with suspension containing 5-nm gold colloids (B, D, F, and H); pit membranes and pit cavities show little accumulation of gold particles. Scale bars = 50 μm .

parenchymatous pit membranes were perforated by numerous plasmodesmata (diameter \approx 100 nm), whereas pores in inter-vessel pit membranes could not be resolved at up to 100,000 \times magnification (Schmid and Machado, 1968).

However, the air seeding hypothesis and the existence of pores large enough to facilitate it are supported by strong corroborative evidence from a number of techniques. These include microscopic observation of *Sphagnum* spp. halocysts (Lewis, 1988), comparison of air injection and water stress-induced vulnerability curves (Cocharde et al., 1992; Sperry and Saliendra, 1994), and reduction of hydraulic conductance by dextrans (Van Alfen et al., 1983) or latex nanospheres (Jarbeau et al., 1995). There is a strong

implication from these studies that pores in the range capable of permitting air seeding exist in most of the inter-vessel pit membranes. For example, experiments which estimate pore size from reduction of hydraulic conductance by dextrans or spheres (Van Alfen et al., 1983; Jarbeau et al., 1995) require that the majority of membranes contain pores that are close to the defined range of particle sizes.

The results from the present study suggest that the vulnerability to embolism of the species examined was not determined by pore sizes intrinsic to the construction of the pit membranes. Rather, it may have more to do with the existence of rare, large pores resultant from weak or damaged membranes. As xylem vessels reach maturity, the protoplast is

destroyed. At the same time, inter-vessel pit membranes are partially hydrolyzed, removing a proportion of the noncellulosic substances (Butterfield and Meylan, 1982). There is some evidence that the pit membranes may undergo further degradation with age, perhaps via the release of pectinase, increasing their porosity. Sperry et al. (1991) showed that pit membranes from young, functional vessels of *Populus tremuloides* often lacked conspicuous pores; but in older vessels, the membranes became increasingly fragile, and large pores ($\approx 0.5 \mu\text{m}$) were observed. There is also evidence that pit membranes might become more "leaky," i.e. damaged or stretched, after cycles of cavitation and refilling (Hacke et al., 2001). Harvey and van den Driessche (1997) stated that drought-resistant hybrid poplar clones possessed stronger pit membranes than drought-sensitive clones, as indicated by the increased damage suffered by membranes during preparation for SEM.

It is important to note that air seeding would require only one large pore per vessel in the thousands of pit membranes that potentially connect embolized and functional vessels. If air seeding were facilitated by damage to a single-pit membrane, it would be extremely difficult to detect by either SEM or exclusion of gold particles. The process of preparation for SEM inevitably damages a large proportion of membranes, and it is impossible to survey all of the pit membranes in a given sample. For particle perfusion experiments, the amount of gold penetrating a single damaged membrane would be very difficult to detect in perfusate. Results from MS of perfusate revealed a very small percentage of particles from 20-nm colloid suspensions penetrated membranes in two of the species. This could be interpreted as evidence of a small number of pores larger than 20 nm, or of the existence of an occasional damaged membrane. However, it could signify that within the distribution of particle sizes in 20-nm colloid suspensions, there exists a fraction of the smaller diameter particles that passed through the membranes. ICP-MS unfortunately does not allow us to differentiate between particle sizes.

CONCLUSIONS

Our results were not consistent with the belief that the natural porosity of pit membranes is linked to a trade-off between safety and efficiency, i.e. that pore size for a given species represents a balance between the increased possibility of air seeding inherent in larger pores and the overall drop in k_h associated with smaller pores (Jarbeau et al., 1995). The trade-off theory suggests that during the construction of pit membranes (primary cell walls), cellulose microfibrils are arrayed in such a fashion that after cell expansion and hydrolysis, pore sizes characteristic of a given species' vulnerability to embolism are present in each membrane. Therefore, the genetics controlling pit membrane porosity would be under

strong selective pressure in plants subjected to water stress (Tyree et al., 1994). However, intact pit membranes of the species examined in our study did not exhibit pore sizes predicted from vulnerability curves. The pressure required to draw a gas bubble through pore sizes observed in the intact membranes would have been at least 14.5 MPa in each of the species.

The discrepancy between air seeding pressures and observed pit membrane porosity could be explained by three possibilities. First, vulnerability to embolism might not have been determined by the natural porosity of pit membranes. Rather, it may be related more closely to the strength and durability of pit membranes, which would determine the frequency with which they are likely to be damaged. Thus, it is possible that natural damage or degradation of membranes may have produced pores of greater size, allowing penetration of gas at smaller pressure differences. Second, pit membrane porosity might be increased by stretching or flexing of the membranes in response to pressure differences between embolized and functional vessels (Hacke and Sperry, 2001; Stiller et al., 2002). Thus, our measurements of the porosity of membranes in a relaxed state would not represent the porosity of the membranes at the point of air seeding. However, this explanation seems unlikely for at least two of the species studied. In *Cochlospermum gillivraei*, the increase in average pore size from between 5 and 20 nm to 200 nm required for air-seedling seems too great to occur by either stretching of the pit membranes or disruption of pectin bridges between microfibrils. The other species, *Austromyrtus bidwillii*, possessed vested pits that filled the pit cavity and would have prevented membranes from stretching significantly in response to pressure differences between embolized and functional vessels. Third, if pores of the required size range were not present, cavitation may have been nucleated by mechanisms other than air seeding, e.g. from vapor embryos in hydrophobic cell wall interstices (Pickard, 1981), although good agreement between vulnerability curves obtained from air injection and dehydration/centrifuge methods indicates this may not be the case in other species.

MATERIALS AND METHODS

Study Site and Plant Species

The study was undertaken in a seasonally dry rainforest community growing in north Queensland at Many Peaks Range, an area on the north-eastern coast of Australia ($19^\circ 11' \text{ S}$, $145^\circ 45' \text{ E}$). Four dry rainforest tree species were selected for the study: two drought deciduous species, *Brachychiton australis* (Schott and Endl.) A. Terracc. and *Cochlospermum gillivraei* Benth., and two evergreen species, *Alphitonia excelsa* (Fenzl) Benth. and *Austromyrtus bidwillii* (Benth.) Burret. All samples used in this study were collected in the wet season, after leaves of the deciduous species were fully expanded (January–March).

Vulnerability Curves

The vulnerability to xylem embolism of each species was measured as the k_h versus the Ψ_x of dehydrated stem segments (Sperry et al., 1988). Branch sections 10 to 30 mm in diameter and longer than the longest vessel length were collected from the field before dawn. After being cut from the trees, they were placed immediately into plastic bags containing wet tissue paper and tightly bound with elastic bands. Upon return to the laboratory, they were removed from the bags and allowed to dehydrate under laboratory conditions (22°C and 60% relative humidity) for between 0 and 10 d. The night before testing was to occur, branches were placed in tightly sealed bags to allow equilibration of water potential (Ψ) throughout the segment and leaves.

On the day of testing, the Ψ of three leaves distal to the segment were measured using a pressure bomb (Plant Moisture Stress, Corvallis, OR). The branch was then recut under water and fitted to a conductivity measurement apparatus. A solution of degassed, 10 mM KCl (pH of 6.5) filtered to 0.22 μm was used for perfusion of branch samples. The PLC was calculated as the difference between the original measurement of k_h at low pressure (≈ 10 kPa) and the maximum value of conductivity (k_{max}) obtained after a series of high pressure flushes (100 kPa for 30 min) from the equation

$$\text{PLC} = 100 (k_{\text{max}} - k_h) / k_{\text{max}} \quad (2)$$

Paired measurements of Ψ_x and PLC were then plotted to determine the vulnerability to embolism of each species with increasing xylem tension.

The data from vulnerability curves were fitted with an exponential sigmoidal equation

$$\text{PLC} = 100 / (1 + \exp\{a[\Psi_x - b]\}) \quad (3)$$

where a and b are constants derived from a linear transformation of Equation 3: $\ln(100/\text{PLC} - 1) = (a\Psi_x - ab)$ (Pammenter and Vander Willigen, 1998). The values of a and b were used to characterize the slope of the line (a) and the value of Ψ_x corresponding to a PLC_{50} (b).

Vessel Anatomy

The diameter and maximum length of xylem vessels were characterized for each species. Vessel diameters were measured from transverse sections of xylem tissue taken from branch samples (10–30 mm in diameter) harvested from the field site. Three branches were taken from three replicates of each species ($n = 9$). Transverse sections of the branches were made, and at least 50 vessels were measured in each of the samples. Digital images were taken of each of the sections from a light microscope and later analyzed using Scion Image (Scion Corporation, Frederick, MD).

The maximum vessel length of three to five branches of each species was measured using low pressure air injection (Zimmermann and Jeje, 1981). The distal end of branch sections was placed under water while air was supplied at the proximal end at a pressure of 100 kPa. Sections 1 cm in length were cut from the submerged end until the first bubbles appeared in the water.

Pit Membrane Porosity

The expected size range of pit membrane pores was calculated for each species from vulnerability curves using Equation 1. The calculated porosity of pit membranes was tested by two methods. First, pit membranes were observed by SEM. Tangential longitudinal and radial longitudinal sections of xylem tissue from branch segments 10 to 30 mm in diameter were cut by hand under a stereo dissector microscope using microtome blades. Sections were cut from the outer layers of xylem tissue (last 1–2 years growth). Sections were air dried for 2 d, affixed to stubs, and coated with platinum before observation. Sections were viewed under a scanning electron microscope (S4500 FESEM, Hitachi, Tokyo) at 35,000 to 50,000 \times magnification.

Second, pit membrane porosity was tested by perfusing suspensions of different sized particles through branch segments of each species. Two different suspensions of gold colloids (100 $\mu\text{L L}^{-1}$ as HAuCl_4 ; Sigma-Aldrich, St. Louis) were used in the experiments; average particle diameter of 20 nm (± 3.0 nm; lot no. 30K91901) and average particle diameter of 5 nm

(± 1.5 nm; lot nos. 120K92451 and 49H91611). Three branches of each species were tested for each particle size.

Branch segments longer than the longest vessel and 10 to 30 mm in diameter were harvested before dawn and were immediately placed in plastic bags containing moist paper tissue. The sections were then transported to the lab which took between 15 to 30 min. The sections were recut under tap water, trimmed at each end with a razor blade and transferred to the k_h apparatus. The system was modified by the addition of a three-way stopcock that allowed for the introduction of the particle suspensions.

Samples were flushed with the perfusing solution described above (0.22 μm filtered, degassed, 10 mM KCl) for 30 min at 100 kPa to remove air emboli from xylem tissue before the introduction of test suspensions. After the flush, 5 mL of gold colloid suspension was introduced to the branch segment via the three-way stopcock. The stopcock was then turned back to the pressure source, and the gold suspension was flushed through the stem section at 100 kPa for 30 min; by this time, all of the colloid suspension, which was pink to reddish brown in color, had moved into the branch segment. Perfusate (≈ 5 mL) was collected from the distal end of the section at varying time intervals (1, 2, 5, 15, 30, and 60 min) after the introduction of the gold suspension.

Perfusate samples were inspected visually for evidence of gold particles penetration through pit membranes. To confirm visual inspections, the perfusate was analyzed using ICP-MS (VG PlasmaQuad, Fison Instruments, UK). ICP-MS is a highly sensitive form of MS used in the analysis of suspensions or solutions. The instrument has a resolution ranging from the low parts per million to high parts per trillion.

Tangential longitudinal sections were cut by hand through the xylem tissue of each sample branch immediately after testing. Representative samples were also embedded in the fast curing resin, Technovit 3040 (Kulzer, Hanau, Germany) for microtome sectioning. Tangential longitudinal sections were then cut on an ultramicrotome to a thickness of 0.5 to 2.0 μm . All sections were observed under bright field on an axioskop light microscope (Carl Zeiss, Jena, Germany) to determine whether the test suspensions had penetrated inter-vessel pit membranes. Light micrographs were acquired digitally with a high resolution CCD camera (Diagnostic Instruments, Sterling Heights, MI).

ACKNOWLEDGMENTS

We thank Cheng Huang and Rodger Heady of the Australian National University electron microscopy unit for assistance with light and electron microscopy. Joe Wolfe (School of Physics, The University of New South Wales) and Martin Canny (Research School of Biological Sciences, Australian National University) are thanked for advice with experimental work and for assistance with preparation of the manuscript.

Received September 6, 2002; returned for revision October 8, 2002; accepted October 8, 2002.

LITERATURE CITED

- Alder NN, Sperry JS, Pockman WT (1996) Root and stem xylem embolism, stomatal conductance, and leaf turgor in *Acer grandidentatum* populations along a soil moisture gradient. *Oecologia* **105**: 293–301
- Butterfield BG, Meylan BA (1982) Cell wall hydrolysis in the tracheary elements of the secondary xylem. In P Baas, ed, *New Perspectives in Wood Anatomy*. Junk Publishers, The Hague, The Netherlands
- Cochard H, Cruziat P, Tyree MT (1992) Use of positive pressures to establish vulnerability curves: further support for the air-seeding hypothesis and implications for pressure-volume analysis. *Plant Physiol* **100**: 205–209
- Crombie DS, Hipkins MF, Milburn JA (1985) Gas penetration of pit membranes in the xylem of *Rhododendron* as the cause of acoustically detected sap cavitation. *Aust J Plant Physiol* **12**: 445–453
- Cronshaw J (1960) The fine structure of the pits of *Eucalyptus regnans* (F. Muell.) and their relation to the movement of liquids into wood. *Aust J Bot* **8**: 51–57
- Dickson WC (2000) *Integrative Plant Anatomy*. Academic Press, San Diego

- Hacke UG, Stiller V, Sperry JS, Pittermann J, McCulloh KA** (2001) Cavitation fatigue: embolism and refilling cycles can weaken the cavitation resistance of xylem. *Plant Physiol* **125**: 779–786
- Harvey HP, van den Driessche R** (1997) Nutrition, xylem cavitation and drought resistance in hybrid poplar. *Tree Physiol* **17**: 647–654
- Jarbeau JA, Ewers FW, Davis SD** (1995) The mechanism of water-stress-induced embolism in two species of chaparral shrubs. *Plant Cell Environ* **18**: 189–196
- Lewis AM** (1988) A test of the air seeding hypothesis using *Sphagnum* halocysts. *Plant Physiol* **87**: 577–582
- Meinzer FC, Clearwater MJ, Goldstein G** (2001) Water transport in trees: current perspectives, new insights and some controversies. *Environ Exp Bot* **45**: 239–262
- Milburn JA** (1993) Cavitation. A review: past, present and future. In M Borghetti, J Grace, A Raschi, eds, *Water Transport in Plants under Climatic Stress*. Cambridge University Press, Cambridge, UK, pp 14–26
- Oertli JJ** (1971) The stability of water under tension in the xylem. *Z Pflanzenphysiol* **65**: 195–209
- Pammenter NW, Vander Willigen C** (1998) A mathematical and statistical analysis of the curves illustrating vulnerability of xylem to cavitation. *Tree Physiol* **18**: 589–593
- Pickard WF** (1981) The ascent of sap in plants. *Prog Biophys Mol Biol* **37**: 181–229
- Schmid R, Machado RD** (1968) Pit membranes in hardwoods-fine structure and development. *Protoplasma* **185**: 185–204
- Shane MW, McCully ME, Canny MJ** (2000) Architecture of branch-root junctions in maize: structure of the connecting xylem and the porosity of pit membranes. *Ann Bot* **85**: 613–624
- Sperry JS, Perry AH, Sullivan JEM** (1991) Pit membrane degradation and air-embolism formation in aging xylem vessels of *Populus tremuloides* Michx. *J Exp Bot* **42**: 1399–1406
- Sperry JS, Saliendra NZ** (1994) Intra-plant and inter-plant variation in xylem cavitation in *Betula occidentalis*. *Plant Cell Environ* **17**: 1233–1241
- Sperry JS, Tyree MT** (1988) Mechanism of water-stress induced embolism. *Plant Physiol* **88**: 581–587
- Stiller V, Sperry JS** (2002) Cavitation fatigue and its reversal in sunflower (*Helianthus annuus* L.). *J Exp Bot* **53**: 1155–1161
- Tyree MT, Davis SD, Cochard H** (1994) Biophysical perspectives of xylem evolution: Is there a trade off of hydraulic efficiency for vulnerability to dysfunction? *IAWA J* **15**: 335–360
- Tyree MT, Sperry JS** (1989) Vulnerability of xylem to cavitation and embolism. *Annu Rev Plant Physiol Mol Biol* **40**: 19–38
- Van Alfen NK, McMillian BD, Turn V, Hess WM** (1983) Role of pit membranes in macromolecular induced wilt of plants. *Plant Physiol* **73**: 1020–1023
- Zimmermann MH** (1983) *Xylem structure and the ascent of sap*. Springer-Verlag, New York
- Zimmermann MH, Jeje AA** (1981) Vessel length distribution in stems of some American woody plants. *Can J Bot* **59**: 1882–1892